Model for fast electrons in ultrashort-pulse laser interaction with solid targets

Wei Yu,[1,2] M. Y. Yu,[1] Z. M. Sheng,[3] and J. Zhang[4]
[1]*Institut für Theoretische Physik I, Ruhr-Universität Bochum, D-44780 Bochum, Germany*
[2]*Shanghai Institute of Optics and Fine Mechanics, Shanghai 201800, People's Republic of China*
[3]*Max-Planck Institut für Quantenoptik, D-85748 Garching, Germany*
[4]*Department of Physics, University of Oxford, Oxford OX1 3PU, United Kingdom*
(Received 5 January 1998; revised manuscript received 25 March 1998)

A simple self-consistent model for the generation of fast electrons during the normal incidence by an ultrashort and ultraintense linearly polarized laser on a solid target is proposed. The electrons are shown to be strongly accelerated in an electron cloud adjacent to the target surface because of resonant interaction with the oscillating component of the ponderomotive force of the laser light. [S1063-651X(98)09908-5]

PACS number(s): 52.40.Nk, 52.35.Mw, 52.60.+h

I. INTRODUCTION

The availability of ultrashort-pulse and ultraintense ($\tau<1$ psec, $I_L\lambda^2>10^{18}$ W μm^2/cm^2, where τ, I_L, and λ are the pulse duration, intensity, and wavelength, respectively) lasers have opened a new physical regime for research on laser-matter interaction. In this regime the laser interaction with solid targets differs significantly from the conventional laser-plasma interactions [1]. Many interesting phenomena [2–10], such as the appearance of high-energy electrons, strong magnetic fields, and high harmonics, etc., have been predicted. Because of its possible application to fast ignition in laser fusion [11], the generation [3–8] of fast electrons is of particular importance.

In the interaction of an ultrashort laser pulse of high contrast with a solid target, ionization occurs very rapidly but the heavy ions have no time to react significantly while the laser is incident. Instead of an expanding plasma corona, the laser field interacts directly with the electrons in the solid-density plasma, with the ions remaining as a positive immobile background. In the ultrastrong laser field the electron motion is highly relativistic, and the electrostatic ponderomotive forces, the time-independent as well as the oscillating components, play important roles. The former determines the density profile of the electrons and the latter drives longitudinal electron oscillations at the second and higher harmonics. In particular, some electrons are pulled out of and sent back into the target by the oscillating field after being accelerated. As pointed out by Wilks [5], for sufficiently large laser intensities, the oscillating ponderomotive field (mainly at the second laser harmonic) leads to an absorption mechanism similar to ''not-so-resonant'' resonant absorption or ''vacuum heating'' [2–5]. However, here oblique incidence of a p-polarized laser light is not required, since the electrons are driven by the oscillating ponderomotive field rather than the normal component of the laser electric field as in the classical vacuum heating.

In this paper a simple self-consistent model describing this scenario is presented. In view of the difficulty associated with the analysis and interpretation of the commonly used Lagrangian approach for the fluid equations, we use a Eulerian formulation, but treat the electrons that are pulled out of and those remaining inside the target separately. The basic features of the model and the results are verified by numerical simulations.

II. PROBLEM DESCRIPTION

We consider the normal incidence of an ultrashort and ultraintense linearly polarized laser pulse on a solid target. As in the earlier works [3,6–8], a steplike density profile is assumed for the immobile ions. The electron density profile is determined self-consistently by the laser field and the electrostatic field of charge separation. The electrons on the target surface are pushed slightly inward by the zero-frequency component of the ponderomotive force, and piled up behind a thin layer of positive ions. At the same time, some electrons are pulled out by the oscillating component of the ponderomotive force. Depending on their initial positions and velocities as well as their interaction history, not all of these electrons will return to the target in the same cycle. Those that remain outside form an electron cloud with a nearly steady-state profile [3,8]. Typically, the electron cloud occupies half a laser wavelength, whereas the penetration (effective skin depth) of the laser into the target is only several percent of the wavelength. Furthermore, the ion layer resulting from the inward compression of electrons is so thin that it can be considered a positive surface charge layer [7]. The electron oscillations (mainly at the second harmonic) driven by the oscillating ponderomotive force are analogous to the electron motion in the capacitor model [4–6,12].

Near the target interface the returning electrons are accelerated by the ''vacuum'' electric fields, which consist of the oscillating ponderomotive field as well as the induced field. In a real vacuum the acceleration of the individual electrons outside the target is relatively weak. Accounting for the electron cloud allows collective phenomena such as resonance to occur. In particular, when the laser is sufficiently intense to create an electron cloud with high enough (near critical) density, the accelerating force in the cloud can become very large. Inside the target, this force rapidly vanishes because of the very high target density. Thus, twice in a laser period trains of electrons strongly accelerated by the resonance reenter the target. These electrons become the high energy component of the total electron population in the solid density plasma. With their stopping distance much larger than

the laser penetration depth, the fast electrons can easily pass the laser penetration layer and deposit their energy deep inside the target.

III. BASIC EQUATIONS

We assume a steplike profile consisting of immobile ions with zero density for $z<0$ and constant density n_i for $z>0$. From the Maxwell's equations we have

$$c^2\nabla^2\mathbf{A}-\partial_t^2\mathbf{A}=4\pi cen\mathbf{u}, \tag{1}$$

$$\partial_t\nabla\phi+4\pi en\mathbf{v}=\mathbf{0}, \tag{2}$$

$$\nabla^2\phi=4\pi e(n-Zn_i), \tag{3}$$

where $\mathbf{u}$ and $\mathbf{v}$ are the transverse and longitudinal components of the electron velocity satisfying $\nabla\cdot\mathbf{u}=0$ and $\nabla\times\mathbf{v}=\mathbf{0}$, $\mathbf{A}$ and ϕ are the vector and scalar potentials satisfying the Coulomb gauge $\nabla\cdot\mathbf{A}=0$, n is the electron density, and Z is the ion charge number.

With the electron thermal velocity much smaller than the quiver velocity, the plasma can be treated as cold [6,7]. As long as the laser spot size is much larger than the depth of laser penetration, one can also assume a planar geometry and write $\mathbf{A}=\mathbf{A}(z,t)$, $\phi=\phi(z,t)$, $\mathbf{u}=\mathbf{u}(z,t)$, and $\mathbf{v}=v(z,t)\hat{\mathbf{z}}$. Substitution of the relativistic Lagrangian $L=-mc^2(1-u^2/c^2-v^2/c^2)^{1/2}-(e/c)\mathbf{u}\cdot\mathbf{A}+e\phi$ of an electron into the Euler-Lagrange equations yields

$$d_t(m\gamma\mathbf{u}-e\mathbf{A}/c)=0, \tag{4}$$

$$d_t(m\gamma v)+(eu/c)\partial_z A-e\partial_z\phi=0, \tag{5}$$

so that $\mathbf{u}=e\mathbf{A}/m\gamma c$. Since usually $|u|\gg|v|$, the relativistic factor becomes $\gamma\sim(1-u^2/c^2)^{-1/2}=(1+a_1^2\cos^2\omega t)^{1/2}$, where $a_1\equiv e|A|/mc^2$ and ω is the laser frequency.

Fourier expanding γ, ϕ, n, and v, e.g., $\gamma(z,t)=\gamma_0(z)+\tilde{\gamma}_2(z,t)+\cdots$, with $\tilde{\gamma}_2(z,t)\equiv\gamma_2(z)\cos 2\omega t$, etc., where

$$\gamma_0=\frac{\omega}{2\pi}\int_0^{2\pi}(1+a_1^2\cos^2\omega t)^{1/2}dt\sim(1+a_1^2/2)^{1/2},$$

$$\gamma_2=\frac{\omega}{\pi}\int_0^{2\pi}(1+a_1^2\cos^2\omega t)^{1/2}\cos 2\omega t dt$$

$$\sim(\gamma_0^2-1)/2\gamma_0,$$

one can obtain from Eqs. (1)–(5) the equations governing the $0\omega,1\omega,2\omega,\ldots$ components of the electron motion. In Sec. IV we shall consider the 0ω and 1ω (the laser field) components, which govern the laser action on the target surface as well as on the electron cloud. In Sec. V we show that the 2ω component of the ponderomotive force can lead to the generation of fast electrons.

IV. ELECTRON DENSITY PROFILE

For the zero-frequency electron motion, the 0ω components of Eqs. (2), (3), and (5) yield $v_0=0$, and

$$\partial_\xi\gamma_0=\partial_\xi\psi_0, \tag{6}$$

$$N-N_i=\partial_\xi^2\psi_0, \tag{7}$$

where $\xi=\omega z/c$, $\psi=e\phi/mc^2$, $N=n_0/n_c$, $N_i=Zn_i/n_c$, and $n_c=m\omega^2/4\pi e^2$ is the critical density.

On the other hand, the 1ω equations yield

$$a_1^{-1}\partial_\xi^2 a_1+1-\gamma_0^{-1}N=0, \tag{8}$$

which is the wave equation for the laser radiation. From Eqs. (6)–(8), we obtain

$$\partial_\xi^2\gamma_0-\gamma_0(\partial_\xi\gamma_0)^2/(\gamma_0^2-1)+(\gamma_0^2-1)(\gamma_0-N_i)=0, \tag{9}$$

where we have made use of the relation $\gamma_0=(1+a_1^2/2)^{1/2}$. Since $\partial_\xi^2\gamma_0=\partial_{\gamma_0}(\partial_\xi\gamma_0)^2/2$, we can self-consistently determine the electron density profile and the other parameters.

A. The target electrons

Under strong laser pressure, the electrons on the target surface are pushed a small distance ξ_b into the target and piled up in a narrow region in $\xi\geqslant\xi_b$, leaving behind a thin layer of ions on the target surface [7,13]. For $\xi\geqslant\xi_b$, the electron density N and the electrostatic field E_0 of charge separation can be obtained from Eqs. (6)–(8). Accordingly, we get

$$N=N_i\gamma_0(3\gamma_0-2)-2\gamma_0(\gamma_0^2-1), \tag{10}$$

$$E_0=(\gamma_0-1)[(\gamma_0+1)(2N_i-\gamma_0-1)]^{1/2}, \tag{11}$$

where we have noted that $E_0=-\partial_\xi\gamma_0$. The electric ($\tilde{E}_1$) and magnetic ($\tilde{B}_1$) fields of the laser light in this region can be expressed as

$$\tilde{E}_1=-\partial_\tau\tilde{a}_1=[2(\gamma_0^2-1)]^{1/2}\sin\tau, \tag{12}$$

$$\tilde{B}_1=\partial_\xi\tilde{a}_1=-\gamma_0[2(\gamma_0-1)(2N_i-\gamma_0-1)]^{1/2}\cos\tau, \tag{13}$$

where $\tau=\omega t$ and $\tilde{a}_1=a_1\cos\tau$. As ξ increases, the electron density N approaches the fixed ion density N_i and the laser field is heavily evanescent.

B. The cloud electrons

In addition to the zero-frequency light pressure, the ponderomotive force contains oscillating electrostatic components at the even harmonics of the laser light. Some plasma electrons in the target will be pulled out by this oscillating ponderomotive electric field and not all of them will return to the target within the same cycle. The electrons remaining outside form a cloud [3,8] adjacent to the target surface. This electron cloud plays a crucial role in the laser-plasma interaction process.

Equations (6)–(8) can also be used to describe the interaction of the laser with the electron cloud. With $N_i=0$ these equations yield for $\xi<0$

$$N=2\gamma_0(\Gamma_0^2-\gamma_0^2), \tag{14}$$

$$E_0=[(\gamma_0^2-1)(2\Gamma_0^2-1-\gamma_0^2)]^{1/2}, \tag{15}$$

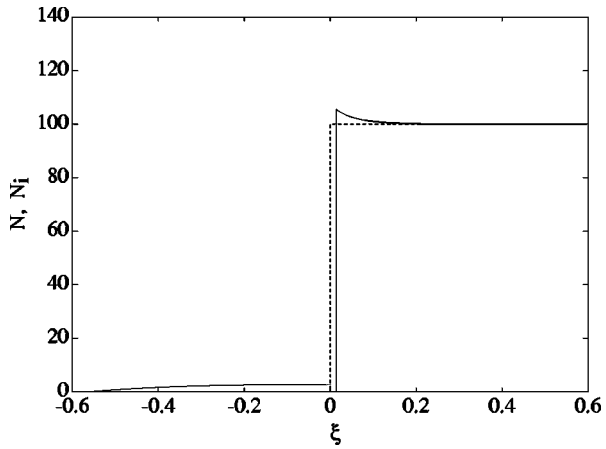

FIG. 1. The electron (solid line) and ion (dashed line) density profiles for $q=1.5$ and $N_i=100$. The electron cloud is included.

$$\tilde{E}_1=[2(\gamma_0^2-1)]^{1/2}\sin\tau, \tag{16}$$

$$\tilde{B}_1=-\gamma_0[2(2\Gamma_0^2-1-\gamma_0^2)]^{1/2}\cos\tau, \tag{17}$$

where Γ_0 is the value of γ_0 at the outer (vacuum side) edge of the electron cloud at $\xi=\xi_a$, where $N=0$. At $\xi=\xi_a$ the boundary conditions require $E_1^2+B_1^2=4B_L^2$, which gives $\Gamma_0^4=2q^2+1$. Here, E_1 and B_1 are the amplitudes of $\tilde{E}_1$ and $\tilde{B}_1$, B_L is the amplitude of the incident light, $q=0.85\times10^{-9}\lambda\sqrt{I_L}$ is the laser strength parameter, where $I_L=(c/8\pi)B_L^2$ is in W/cm^2 and λ in μm.

C. The positive layer

The immobile ions in the positively charged layer have no effect on the electromagnetic fields, so that $E_1(0)=E_1(\xi_b)$ and $B_1(0)=B_1(\xi_b)$, which give $\Gamma=1+(\Gamma_0^2-1)/N_i$, where Γ is the value of γ_0 on either side of the positive layer.

The depth of the positive layer can be determined from the charge conservation equation

$$N_i\xi_b=\int_{\xi_a}^{0}Nd\xi+\int_{\xi_b}^{\infty}(N-N_i)d\xi=\Gamma_0^2-1, \tag{18}$$

which gives $\xi_b=(\Gamma_0^2-1)/N_i$. The depth of laser penetration into the plasma, defined as the distance at which the radiation is damped to $1/e$ of its value at the target surface, is given by

$$\xi_d=N_i^{-1/2}[\coth^{-1}(\zeta_d)-\coth^{-1}(\zeta)]+\xi_b, \tag{19}$$

where $\zeta_d^2=[(1+(\Gamma^2-1)/e^2)^{1/2}+1]/2$, $\zeta^2=(\Gamma+1)/2$, and

$$\xi_a=\int_{\Gamma}^{\Gamma_0}[(\gamma_0^2-1)(2\Gamma_0^2-1-\gamma_0^2)]^{-1/2}d\gamma_0 \tag{20}$$

is the size of the electron cloud.

Figure 1 shows the electron (solid line) and ion (dashed line) density profiles for $q=1.5$ and $N_i=100$. Figure 2 shows the q dependence of ξ_a, ξ_b, and ξ_d for $N_i=100$. For solid targets with $N_i\gg1$, the electron cloud occupies about half a laser wavelength, and the laser penetration depth is only several percent of it. The positive layer is thus so small that it can be taken as a surface charge layer [7].

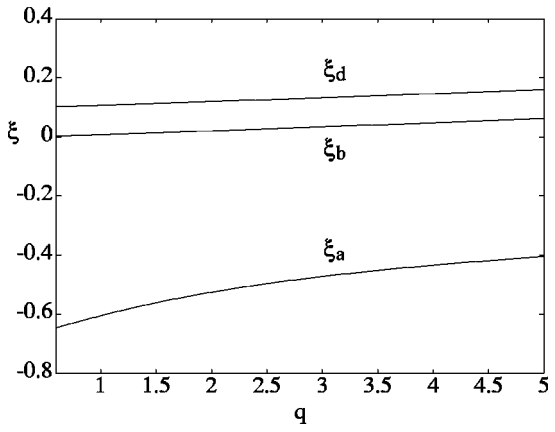

FIG. 2. The q dependence of the depths ξ_a, ξ_b, and ξ_d of the electron cloud, positive charge layer, and laser penetration layer, respectively. For $N_i=100$.

V. FAST ELECTRON GENERATION

From Eqs. (1)–(5) we obtain the governing equations for the electron (Langmuir) oscillations at 2ω

$$N\tilde{V}_2=\partial_\tau\tilde{E}_2, \tag{21}$$

$$\gamma_0\partial_\tau\tilde{V}_2+\partial_\xi\tilde{\gamma}_2+\tilde{E}_2=0, \tag{22}$$

$$\partial_\xi\tilde{E}_2=-\tilde{N}_2, \tag{23}$$

where $\tilde{N}_2=\tilde{n}_2/n_c$, $\tilde{V}_2=\tilde{v}_2/c$, and $\tilde{E}_2=-\partial_\xi\tilde{\psi}_2$. These equations yield

$$\tilde{E}_2=\tilde{E}_p[(1-N/4\gamma_0)^{-1}-1], \tag{24}$$

$$\tilde{V}_2=E_p\sin2\tau/2\gamma_0(N/4\gamma_0-1), \tag{25}$$

where $\tilde{E}_p=E_p\cos2\tau=\partial_\xi\tilde{\gamma}_2$ is ponderomotive field, $E_p=(\gamma_0^2+1)(\partial_\xi\gamma_0)/2\gamma_0^2$. The driven Langmuir oscillation is formally analogous to that in the often invoked capacitor model [12] if we consider $\tilde{E}_p$ as a nonuniform driver and $\epsilon=1-N/4\gamma_0$ as a relativistic dielectric function.

Figure 3 shows the ξ dependence of the ponderomotive field $\tilde{E}_p$ (dotted curve), the induced field $\tilde{E}_2$ (dashed curve), as well as the total electric field $\tilde{E}_2+\tilde{E}_p$ (solid curve) at $\cos2\tau=-1$ for $N_i=100$ and $q=1.5$. Figure 4 shows the amplitude of the corresponding oscillation velocities.

The electron density profile obtained in Sec. IV represents a configuration favorable for the production of energetic electrons. The electron cloud preceding the target allows resonance to occur, leading to a strong accelerating field. The amplitude of the Langmuir oscillation can become very large, especially when the cloud density is close to resonance (i.e., $N\to4\gamma_0$). Twice in a laser period (when $\sin2\tau=-1$), trains of the accelerated electrons stream into the target. Their density and velocity are given by

$$N(0_-)=2\Gamma(\Gamma_0^2-\Gamma^2), \tag{26}$$

$$V_2(0_-)=(\Gamma^2+1)[(\Gamma^2-1)(2\Gamma_0^2-\Gamma^2-1)]^{1/2}R, \tag{27}$$

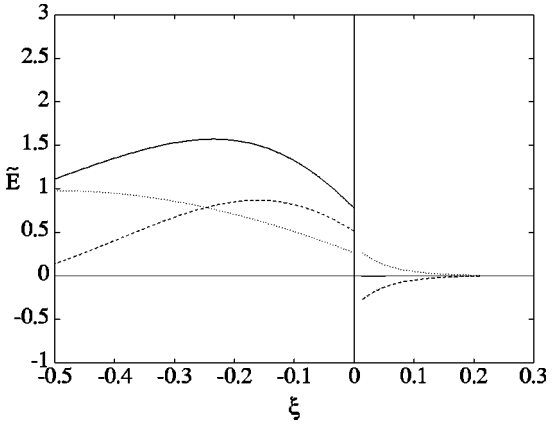

FIG. 3. The ξ dependence of the ponderomotive field $\tilde{E}_p$ (dotted curve), induced field $\tilde{E}_2$ (dashed curve), and the total electric field $\tilde{E}_2+\tilde{E}_p$ (solid curve) at $\cos 2\tau=-1$ for $N_i=100$ and $q=1.5$.

where $R\equiv\Gamma^{-2}[N(0_-)-4\Gamma]^{-1}$ is the resonance factor which gives rise to large $V_2(0_-)$. We note that without the electron cloud, the accelerating field would just be $\tilde{E}_p$ (i.e., $\tilde{E}_2=0$) and the resulting electron oscillation velocity would be much smaller (see Figs. 3 and 4).

Inside the target the induced field, which is in the opposite direction, tends to repel the fast electrons. However, for solid targets with $N_i\gg 1$ this induced field is greatly depressed as it is almost canceled by E_p. In fact, the total field almost vanishes (the solid line in Fig. 3 is nearly overlapped by the ξ axis). Thus, the velocity oscillations of the local electrons (those not pulled out of the target) are very small and the electrons do not go beyond the thin laser-penetration layer. Furthermore, the incoming high-speed electrons (dashed line in Fig. 4) are almost unaffected by the small electric field inside and can therefore penetrate deep into the target. On the other hand, because of the very high density of the local electrons, the high-speed electrons returning from the electron-cloud side constitute only a small fraction of the total electron population inside the target.

VI. DISCUSSION

It has been often been suggested that the electrons returning from the vacuum side would intersect trajectories *inside*

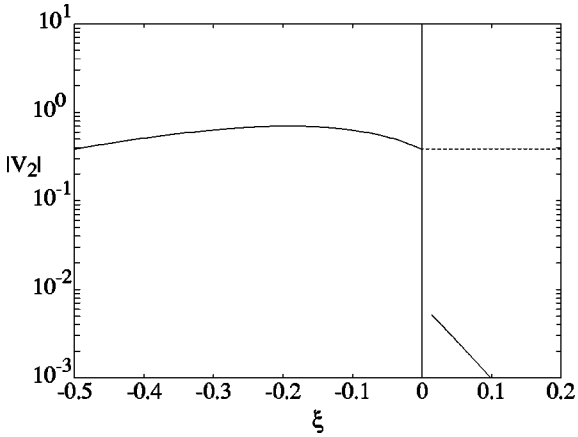

FIG. 4. The ξ dependence of the amplitude of the 2ω oscillation velocity at $\sin 2\omega t=-1$ for $N_i=100$ and $q=1.5$.

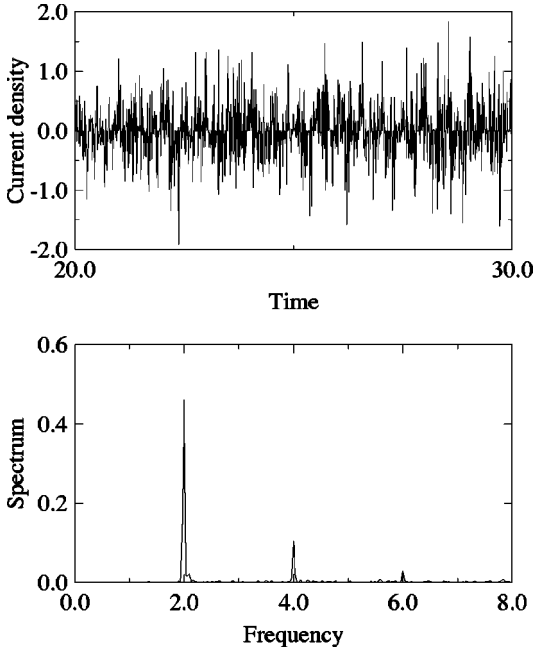

FIG. 5. Results at $\xi=0_-$ from numerical simulations, for laser strength parameter $q=2$ and normalized target density $N_i=100$. (a) The time evolution of the normalized electron current density nv/n_cc. (b) The corresponding frequency spectrum. The frequency axis is in units of the laser frequency ω and the spectrum is in arbitrary units.

the target and result in wave breaking and generation of high energy electrons. In the present picture, due to the unique density structure in the interaction of an ultrashort-pulse and intense laser with solid density plasmas, some of the electrons pulled out of the target are in fact resonantly accelerated in the electron cloud and driven back into the target. For $N_i\gg 1$, the range of the fast electrons greatly exceeds the

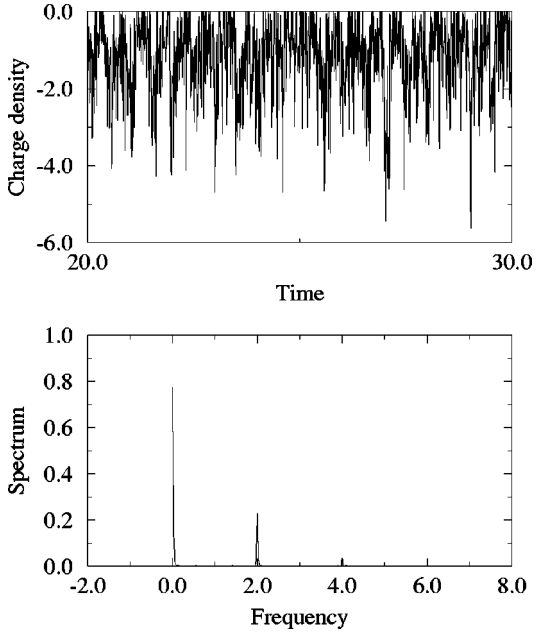

FIG. 6. Same parameters as in Fig. 5. (a) The time evolution of the normalized electron charge density $-n/n_c$. (b) The corresponding frequency spectrum.

depth of laser penetration. These very fast electrons easily pass through the laser penetration layer with little or no interaction with the local electrons. Thus most of their energy will be deposited deep inside the target through collisions.

According to Eq. (25), as $q \to 2[N_i(N_i-1)]^{1/2}/(N_i-2)$, the cloud density $N \to 4\gamma_0$ and the fast-electron flow will greatly increase. However, when $v_2 \to c$ the assumption $|u| \gg |v|$, and hence our analytical model, are no longer valid. In this case the approximation $\gamma \sim (1+a_1^2\cos^2\omega t)^{1/2}$ must be replaced by the exact expression $\gamma=(1-u^2/c^2-v^2/c^2)^{-1/2}$, and the analysis is no longer straightforward. To consider this case as well as to verify the assumptions in our model, numerical simulations for $q \geqslant 2[N_i(N_i-1)]^{1/2}/(N_i-2)$ are performed using the LPIC++ code [14]. Since there exist many recent simulations of the interaction of intense lasers with high-density plasmas, here we discuss only the results for the electron behavior just in front of the target.

Figure 5 shows the time evolution of (a) the frequency spectrum, and (b) the electron current density at $\xi=0_-$ for $q=2$ and $N_i=100$. Figure 6 shows the corresponding plots for the electron charge density. The strong 0ω peak in the density spectrum (but not in the charge density spectrum) confirms the existence of an electron cloud just outside the target. The rapidly decreasing peaks at the higher (even-order) harmonics in both spectra indicate that the longitudinal electron current density at $\xi=0_-$ is dominated by the 2ω component, so that the Fourier expansion in our model is justified. As a result, trains of electrons are driven into the target every half laser period with high but finite velocities. Such fast electrons are indeed seen in the corresponding phase space, as have already been found in the existing simulations [3–5]. In the earlier simulations of normally incident p-polarized light of lower q values, no noticeable amount of 2ω ponderomotive oscillations were found, and there is correspondingly no significant fast electron generation.

Finally, it is of interest to point out that in our simulations (not shown) for even larger q, both the electron cloud density and the 2ω oscillations increase as expected, and electrons with higher and higher velocities appear. However, it seems that, probably because of the relativistic effect mentioned above, by increasing the laser intensity one can approach the resonance condition but not actually reach it.

ACKNOWLEDGMENTS

We thank R. Lichter, R. E. W. Pfund, and J. Meyer-ter-Vehn for useful discussions and their LPIC++ code that we used in our simulations. This work was partially supported by the Sonderforschungsbereich 191 Niedertemperatur Plasmen. One of the authors (W.Y.) would like to thank the K. C. Wong Education Foundation, the Deutscher Akademischer Austauschdienst, and the National High-Technology Program of China (Contract No. 863-416-3-1-4) for financial support.

[1] C. E. Max, Lawrence Livermore National Laboratory Report No. UCRL-53107.
[2] F. Brunel, Phys. Rev. Lett. **59**, 52 (1987).
[3] P. Gibbon and A. R. Bell, Phys. Rev. Lett. **68**, 1535 (1992).
[4] S. C. Wilks, Phys. Rev. Lett. **69**, 1383 (1992).
[5] S. C. Wilks, Phys. Fluids B **5**, 2603 (1993).
[6] S. Kato, B. Bhattacharyya, A. Nishiguchi, and K. Mima, Phys. Fluids B **2**, 564 (1993).
[7] R. N. Sudan, Phys. Rev. Lett. **70**, 3075 (1993).
[8] S. V. Bulanov, N. M. Naumova, and F. Pegoraro, Phys. Plasmas **1**, 745 (1994).
[9] P. A. Norreys, M. Zepf, S. Moustaizis, A. P. Fews, J. Zhang, P. Lee, M. Bakarezos, C. N. Danson, A. Dyson, P. Gibbons, P. Loukakos, D. Neely, F. N. Walsh, and J. S. Wark, Phys. Rev. Lett. **76**, 1832 (1996).
[10] G. Malka and J. L. Miguel, Phys. Rev. Lett. **77**, 75 (1996).
[11] M. Tabak *et al.*, Phys. Plasmas **1**, 1676 (1994).
[12] G. J. Morales and J. C. Lee, Phys. Rev. Lett. **33**, 1016 (1974); *ibid.* **33**, 1534 (1974).
[13] C. S. Lai, Phys. Rev. Lett. **36**, 966 (1976).
[14] R. Lichter, R. E. W. Pfund, and J. Meyer-ter-Vehn, MPI Quantenoptik, Garching, Report No. MPG225, 1997.